An Attempt to Estimate the Sulfuric Acid Dewpoint in the Flue Gas from Aluminium Electrolysis Cells

Asbjørn Solheim

SINTEF, P.O. Box 4760 Torgarden, NO-7465 Trondheim, Norway

Key words: Flue gas, Gas composition, Crust opening, Dewpoint

Abstract

The sulfuric acid dewpoint in the flue gas from aluminium electrolysis cells increases with increasing concentrations of sulfur dioxide and water vapour. This represents a potential problem in a future scenario with reduced air draught for increased carbon dioxide capture and heat exchangers for cooling or heat collection. A pragmatic model was derived, based on kinetics for the sulfur dioxide to trioxide conversion and models for estimating the temperature and air penetration into the flame. The results indicate that oxidation of carbon monoxide as well sulfur dioxide takes place mainly less than 10 cm above the crust opening. The dewpoint increases with decreasing current efficiency and with increasing area and diameter of the crust openings. In the base case, which was thought to be representative for a modern prebake cell, the dewpoint was 73 °C. The dewpoint may increase if sulfur trioxide is refluxed with the secondary alumina.

1 Introduction

Corrosion due to sulfuric acid is a challenge in many combustion processes. The sulfur present in the fuel primarily forms SO_2, which is partly oxidized to SO_3. Gaseous sulfuric acid (H_2SO_4) is formed by reaction between SO_3 and water vapour, and the acid will condense if the local (wall) temperature is below the sulfuric acid dewpoint. The acid dewpoint temperature increases with increasing concentrations of water vapour and SO_3. The degree of conversion of SO_2 to SO_3 is a key point. It is usually a few percent in fossil fuel fired power plants, and the reaction is known to be catalysed by substances present in fly ash.

An aluminium cell contains all the factors necessary to form sulfuric acid. The sulfur concentration in the petrol coke used for making anodes may be up to 6 wt% (the amount is currently increasing due to deteriorating quality of the coke). There is a positive correlation between the concentrations of sulfur and vanadium [1], and vanadium oxide is known to catalyse the SO_2 to SO_3 conversion [2]. Furthermore, there is high temperature above the crust openings due to combustion of CO with air. Water is always present in the secondary alumina as well as in the huge amounts of air sucked into the cell for cooling and keeping sufficient underpressure inside the superstructure. Still, the sulfuric acid dewpoint does not seem to be a serious concern in the aluminium industry; in fact, the dewpoint of the flue gas is hardly mentioned in the open literature. Presumably, this reflects that the dewpoint is so low that the problem is largely avoided. More specific; the degree of SO_2 to SO_3 conversion is probably very low.

It is likely that carbon capture and sequestration (CCS) will become an integrated part of many industrial processes in the future. For the aluminium industry, this entails that the concentration of CO_2 in the flue gas must be substantially increased from the current 1 vol%, meaning that the air draught must be reduced. A device for reducing the draught without compromising the hooding efficiency has already been developed [3]. Recycling of the flue gas in order to reduce the amount of "fresh" air was patented by GE Power [4, 5], and the idea was recently discussed by Solheim and Senanu [6]. Reduced draught as well as recycling gives higher concentration of CO_2 (the concentration is approximately inversely proportional with the air flow), but also the concentration of other process gases, such as HF and SO_2, increase in the same manner. Moreover, reduced draught and gas recycling will require heat exchangers; this is in order to protect vital components in the superstructure, and to keep the flue gas temperature suitable for efficient scrubbing. Utilization of recovered heat is also a part of future scenarios for the aluminium industry. Inevitably, a heat exchanger presents a cold surface where formation of sulfuric acid can occur. All in all, it seems probable that the future will bring increased dew point temperatures and reduced wall temperatures.

The main part of the present work is the estimation of the degree of SO_2 to SO_3 conversion in aluminium electrolysis cells. While the modelling approach can be regarded as simplistic and the absolute values given are very uncertain, it is believed that the variation with the different parameters may be qualitatively correct.

2 Pragmatic Model. Assumptions and Initial Calculations

2.1 Process Gas Composition. Base Case

A schematic illustration of the Excel-based pragmatic model used in the present work in shown in Fig. 1. The model comprises an opening in the crust, e.g., a feeder hole, where the process gases formed at the anode and underneath the crust flow upwards and mix with air inside the cell superstructure. The mixing and reaction zone shown in Fig. 1 was subdivided into 200 elements in the vertical direction, containing increasing amounts of air. It was assumed that all the gas species are well mixed within each element.

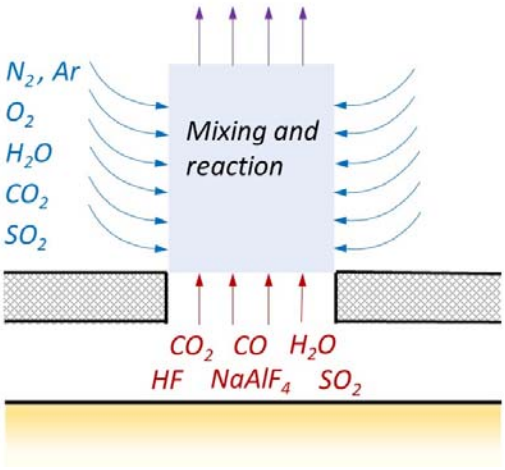

Figure 1. Schematic illustration of the pragmatic model used in the present work.

The molar flows and composition of the anode gas are shown in Table 1. The amounts of HF and $NaAlF_4$ were based on the fluoride evolution model by Haupin and Kvande [7]. The gases were mixed with air composed of 78.16 vol% N_2 and Ar, 20.80 vol% O_2, 1.00 vol% H_2O, and 0.041 vol% CO_2. The total draught was assumed to be 8000 Nm^3h^{-1} in a 400 kA cell, i.e., the total air flow was 98.0 $mols^{-1}$. The enthalpy for combustion of CO with air, as well as the specific heat capacities for the gas species involved, were taken from Knacke et al. [8]. In the base case, the current efficiency (CE) was assumed to be 94 %, the bath temperature was 960 °C, and the initial temperature of the air mixed into the process gas was 110 °C. The process gas was assumed to leave through 6 crust openings (feeder- and tapping holes), each with 0.2 m dia.

Table 1. Gases released and consumed underneath the crust in a 400 kA cell. All numbers are in mol s^{-1}.

	CO_2	CO	HF	H_2O	$NaAlF_4$	SO_2
Main anode reaction	1.0364	-	-	-	-	-
Loss in current efficiency (94% CE)	-0.1244	0.1244	-	-	-	-
Boudouard reaction at anode (15 kg C/t Al)	-0.0438	0.0876	-	-	-	-
Boudouard reaction elsewhere (5 kg C/t Al)	-0.0146	0.0292	-	-	-	-
Moisture from alumina (1.2 wt% H_2O)	-	-	-	0.0440	-	-
Evaporation (11.3 kg $NaAlF_4$/t Al) -	-	-	-	-	0.0031	-
Hydrolysis of bath (12.5 kg HF/t Al)	-	-	0.0210	-0.0105	-	-
Hydrolysis of $NaAlF_4$ (1.7 kg HF/t Al)	-	-	0.0030	-0.0015	-0.0010	-
From sulphur in the anode (2.3 wt%)	-	-	-	-	-	0.0110
Sum molar flows	0.8536	0.2412	0.0240	0.0320	0.0022	0.0110
Composition of process gas [vol%]	73.34	20.72	2.06	2.75	0.18	0.95

2.2 *Initial Calculations: Gas Composition and Temperature*

The CO formed by loss in current efficiency (CE) and in the Boudouard reaction will partly be consumed above the crust openings by combustion with to form CO_2. The reaction is important in the present work, since it determines the temperature in the gas on its way out. Many sources indicate a lower flammability limit (LFL) of CO of 12-12.5 vol% at room temperature, but it decreases with increasing temperature. Zlochower [9] indicated that the LFL is about 7.7 vol% CO at 450 °C. The first test of the model was to study the effect of the LFL on the CO/CO_2 ratio in the flue gas. Data compiled by Aarhaug and Ratvik [10] indicate that this ratio is about 0.1 in industrial cells. It was assumed that the combustion rate (r_{CO}) depends on the product of the CO concentration and the square root of the O_2 concentration (since the reaction proceeds with oxygen radicals, $O\cdot$), and that it decreases rapidly as the CO concentration approaches the LFL. The following was derived by trial and error:

$$r_{CO} = -1.4 \cdot 10^{-4} \cdot p_{CO} \cdot p_{O_2}^{1/2} \cdot exp(-[0.06/p_{CO})]^3) \qquad [\text{molm}^{-3}\text{s}^{-1}] \tag{1}$$

where p is the partial pressure in atm. The exponential term in Eq. 1 implies that the reaction slows down rapidly when the CO pressure approaches 0.06 atm, which was the assumed LFL. The amount of CO reacted in one element was calculated by

$$\Delta n_{CO} = r_{CO} \cdot A \cdot \Delta z \qquad [\text{mols}^{-1}] \tag{2}$$

where A is the total cross-sectional area of the crust openings and Δz is the height of the element. The concentrations and the temperature were calculated in terms of the amount of air mixed into the process gas. The relationship between air flow and vertical distance was estimated by an equation for air penetrating into an open flame [11]:

$$m_{air} = 1.24 \cdot z^{3/2} \cdot d \quad [\text{kgs}^{-1}] \tag{3}$$

where m_{air} is the air mass flow, z is the distance from the base of the flame, and d is the diameter of the base (in this case, the crust opening).

Calculation of the temperature of the process gas and air mixture involved balancing the enthalpy from the combustion of CO and the change in heat content of the process gas and air. It was found necessary to adjust the temperature for heat loss by radiation, since gas mixtures containing molecules with more than two atoms emit thermal radiation. The emissivity (ε) of a gas depends on the product of the partial pressure (p) of the radiating species and the dimension of the gas body (L). The emissivities for gas mixtures containing CO_2 and H_2O is shown in Thirumaleshwar [12]. At 1200-1500 K and $p \cdot L$ in the range of 0.01 to 0.2 m · atm it was decided to use an efficient emissivity $\varepsilon_{eff} = 0.06$ in the entire range. The thermal radiation was assumed to take place from a cylinder with diameter corresponding to the crust opening and height of half the diameter. The radiation was assumed to take between the gas and the bath (T_b = 1233 K) through the base of the cylinder, and between the gas and the surroundings through the side and top of the cylinder. The "effective" temperature of the surroundings (T_{eff}) was assumed to be 100 K higher than the final gas temperature in the superstructure to account for the higher temperatures in the nearby anode assemblies. The radiative heat loss from one opening becomes

$$Q_{rad} \approx \left[(T_{av}^4 - T_b^4) \cdot \sigma \cdot \frac{\pi}{4} d^2 + (T_{av}^4 - T_{eff}^4) \cdot \sigma \cdot \frac{3\pi}{4} d^2\right] \cdot \varepsilon_{eff} \qquad [\text{W}] \tag{4}$$

where T_{av} is the average gas temperature inside the volume defined by the cylinder and σ is the Stefan-Bolzmann constant [$5.67 \cdot 10^{-8}$ $\text{Wm}^{-2}\text{K}^{-4}$]. The average gas temperature was evaluated as

$$T_{av} = (\sum T^4/N)^{1/4} \tag{5}$$

where N is the number of elements within $z < d/2$. The heat loss was distributed uniformly from the gas inside the volume limited by $z \leq d/2$.

The gas composition at 94 % CE (process gas composition in Table 1) is shown as a function of the amount of entrained air in Fig. 2. The gas temperatures with different CEs is shown in Fig. 3. Fig. 4 shows the consumption rate of CO as a function of the air flow rate and the vertical position. As can be observed, the reaction is finished after about 10 cm.

Admittedly, the procedures described above are simplistic. From the data by Zlochover [9], one would expect that the LFL should be somewhat lower than the mentioned 6 vol% at the temperatures prevailing above crust openings.

It is possible that part of the CO is protected by lack of oxygen penetrating into the core of the flame. This may indicate that the "well mixed" condition used in the current model is indeed simplistic. Still, there is some evidence that the model does not produce completely wrong results. The CO/CO_2 ratio of about 0.1 found by Aarhaug and Ratvik [10] was neatly reproduced; the calculated ratio varied almost linearly from 0.087 at 96 % CE to 0.113 at 86 % CE. Moreover, Osen *et al*. [13] measured HF concentration and temperature inside a feeder hole in an industrial cell. Simultaneous values of about 800-850 °C (1073-1123 K) and up to 0.8 percent HF were recorded, which fits well with the data shown in Figs. 2 and 3 at $G/G_{tot} \approx 0.02$ (the exact CE in the cell studied is not known).

The sulfur in the anode was assumed to be present as SO_2 from the very beginning, although the initial compound is probably COS, and SO_2 formation requires the presence of O_2. The SO_2 in the flue gas is partly adsorbed in the dry scrubber and returned to the cell with the alumina. In the base case, it was assumed that 50 percent of the SO_2 is returned to the cell.

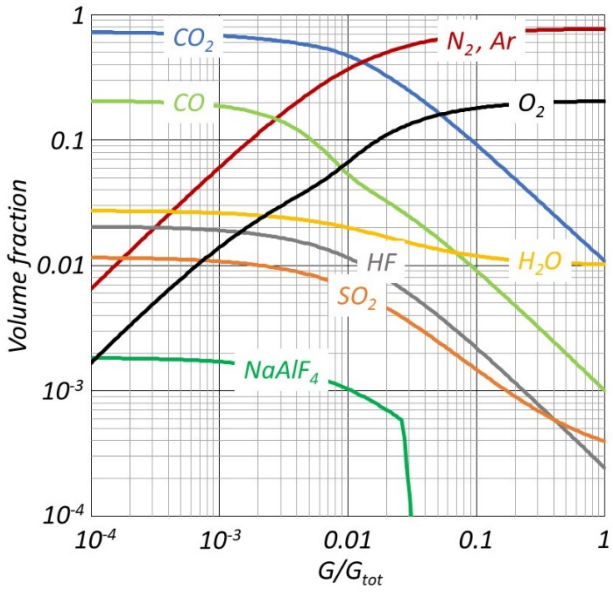

Figure 2. Gas concentrations as a function of the amount of air mixed into the process gas. 94 % CE, LFL = 6 vol% CO.

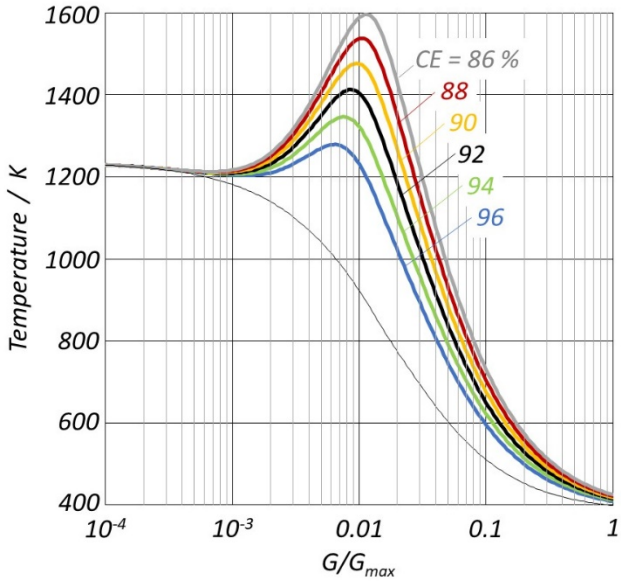

Figure 3. Gas temperature as a function of the amount of air mixed into the process gas. The thin line is the temperature without combustion of CO (only mixing of air and process gas).

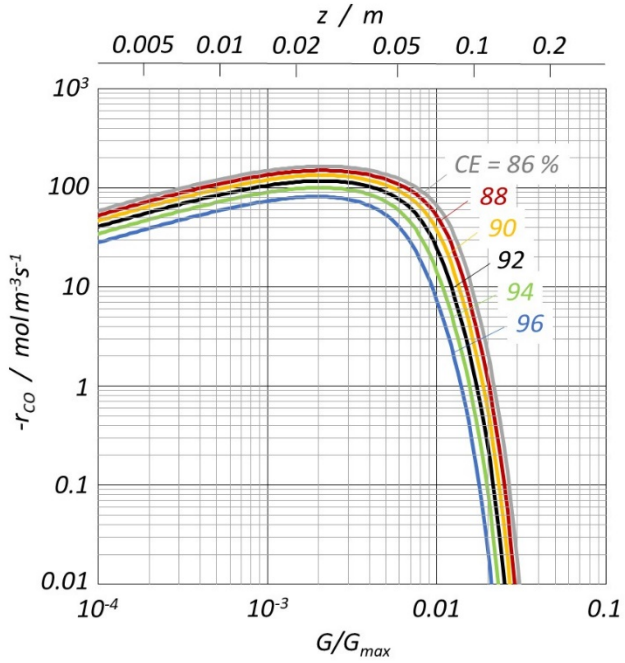

Figure 4. Rate of combustion of CO as a function of the amount of air mixed into the process gas and as a function of the vertical position (upper scale).

3 Sulfur Dioxide to Trioxide Conversion

3.1 Rate Expression. Effect of Current Efficiency

The thermodynamics of SO_3 formation is favourable at low temperature, but the kinetics are slow. The overall reaction

$$SO_2 + \frac{1}{2}O_2 = SO_3 \quad (6)$$

proceeds via the oxygen radical (O·) and a third molecule M (termolecular reaction):

$$SO_2 + O\cdot + M = SO_3 + M \quad (7)$$

The equilibrium between molecular oxygen and oxygen radicals, $O_2 = 2O\cdot$, is strongly temperature dependent. The concentration of radicals is proportional with the square root of the O_2 pressure. The radical concentration was calculated using Gibbs energy taken from NIST-JANAF [14].

The rate (r) of SO_3 formation can be calculated by

$$r_{SO_3} = k \cdot c_{SO_2} \cdot c_{O_2} \cdot c_M \cdot exp\left(\frac{-E_a}{RT}\right) \quad [\text{molm}^{-3}\text{s}^{-1}] \quad (8)$$

where c is concentration [molm^{-3}] E_a is the activation energy, and R is the gas constant [8.3143 Jmol^{-1}K^{-1}]. The "third molecule" M was taken to be all gas species other than O_2 and SO_2. Based on values for the rate constant and activation energy at high temperature listed in NIST Chemical Kinetics Database [15] it was decided to use $E_a = 0$ and $k = 1 \cdot 10^{-32}$ cm^6 · molecule^2 · s^{-1} (3627 m^6 mol^{-2} s^{-1}). The reason for the strong variation of the total reaction rate with temperature is the temperature dependence of splitting of oxygen molecules into radicals.

The degree of SO_2 to SO_3 conversion (ψ) was found by summing up the amount of SO_3 formed in each element and dividing by the amount of SO_2 stemming from the anode:

$$\psi = \frac{\sum r \cdot A \cdot \Delta z}{n^0_{SO_2}} \quad (9)$$

where A is the total cross-sectional area of the crust openings.

The local reaction rates are shown in Fig. 5. The reaction takes place mainly between 5 and 10 cm from the base, and the rate follows the temperature closely (Fig. 3). The total degree of conversion from SO_2 to SO_3 is a strong function of the CE, as shown in Fig. 6.

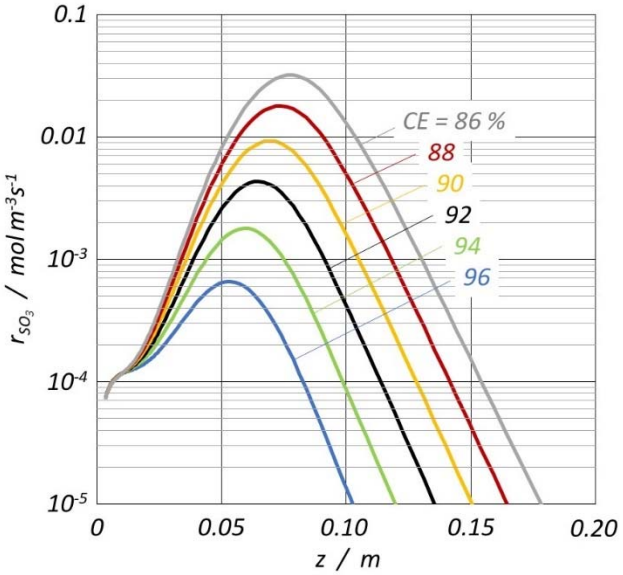

Figure 5. Rate of conversion of SO_2 to SO_3 as a function of the vertical position at different current efficiencies.

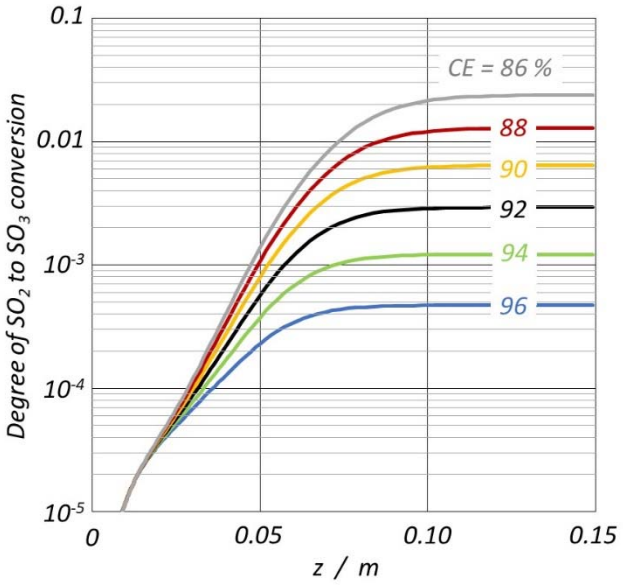

Figure 6. Degree of SO_2 to SO_3 conversion as a function of the distance from the base at different current efficiencies.

3.2 Crust Openings

In the base case (400 kA cell) there were 6 crust openings each 0.2 m dia. The number of openings was varied from 2 to 8, and the diameter was varied from 0.05 to 0.3 m. It turned out that the crust openings had a huge effect on the degree of conversion. Most of the variation can be explained by the residence time of SO_2 in the reaction zone. This time is proportional with the area of the openings (effect of linear velocity), and it will also be approximately proportional with the crust opening diameter d (it follows from Eq. 3 that the rate of air penetration increases with d).

The dotted lines in Fig. 7 represent the SO_2 to SO_3 conversion by the simple function:

$$\psi \propto A_{100} \cdot d \tag{10}$$

where A_{100} is the area of openings per 100 kA cell amperage. In the base case, $A_{100} \cdot d$ = 0.0094 m^3. The data calculated with 94 % CE fit reasonably well with Eq. 10, but the equation overestimates ψ at small $A_{100} \cdot d$, particularly with low CE. It was observed that the CO/CO_2 ratio varied somewhat with the geometry of the openings, which affects the temperature.

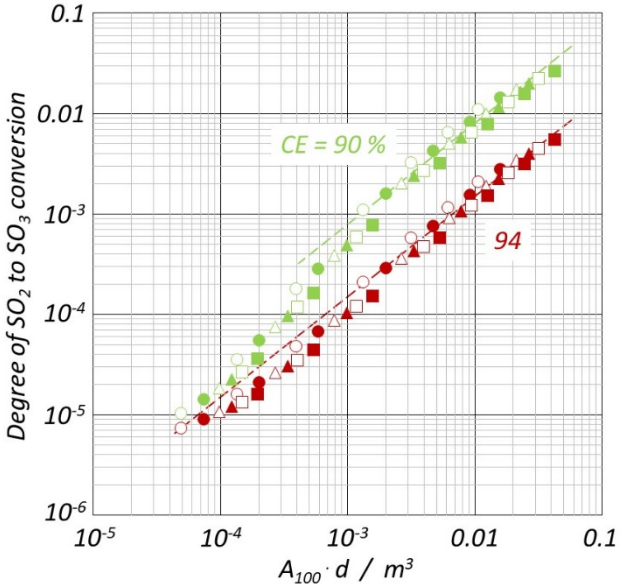

Figure 7. Degree of SO_2 to SO_3 conversion as a function of the product of crust opening area per 100 kA and the representative opening diameter at two current efficiencies. The symbols represent different number of crust openings (2-8 for a 400 kA cell).

3.3 Temperature and Draught

The temperature in the reaction zone is influenced by the bath temperature as well as the temperature of the air inside the superstructure. Figure 8 shows that the effect of temperature is not dramatic.

The temperature in the superstructure increases is the air draught is reduced, but there was virtually no effect of the draught itself when reducing it from 8000 Nm^3h^{-1} to 2000 Nm^3h^{-1}. The reason appears to be that the SO_2 to SO_3 conversion takes place with relatively small amounts of air (from the figures above, all reactions are practically finished at $G/G_{tot} \approx 0.02$, i.e., when 160 Nm^3h^{-1} of air is mixed into the process gas (approximately 94 Nm^3h^{-1} in a 400 kA cell).

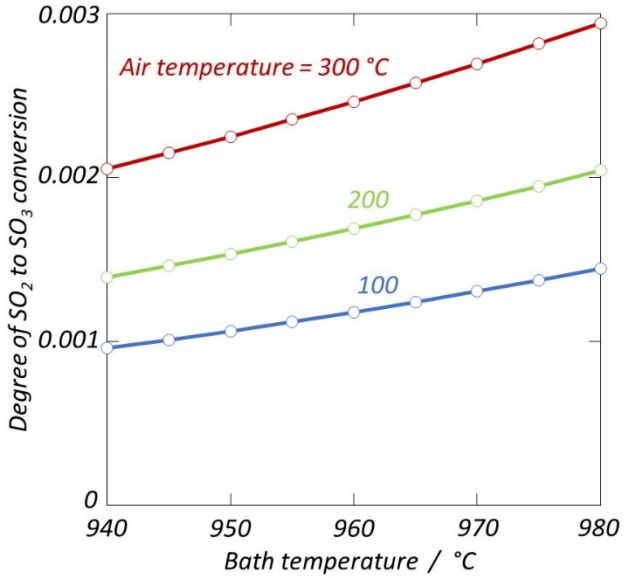

Figure 8. Degree of SO_2 to SO_3 conversion as a function of the bath temperature with different temperatures of air penetrating into the process gas.

4 Sulfuric Acid Dewpoint. Reflux of SO_2 and SO_3

There are several equations for calculating the sulfuric acid dewpoint (θ_{dew}). The equations produce dewpoints usually within 10 °C, and the trends with SO_3 concentration and moisture content are similar. The equation by ZareNezhad and Aminian [17] is used in the present work:

$$\theta_{\text{dew}} = 150 + 8.1328 \cdot \ln(p_{H_2O}) + 11.664 \cdot \ln(p_{SO_3}) - 0.38226 \cdot \ln(p_{H_2O}) \cdot \ln(p_{SO_3}) \quad [°C] \quad (11)$$

where the partial pressures are in mm Hg. The equation is represented graphically in Fig. 9.

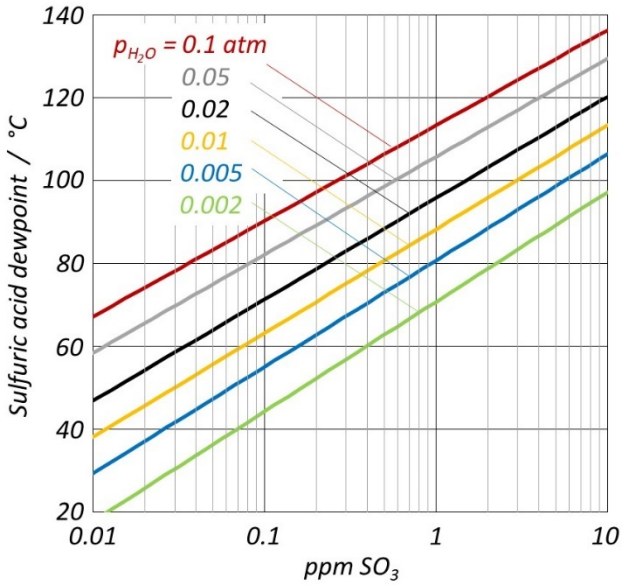

Figure 9. Sulfuric acid dew point as a function of the concentration of SO_3 at different water vapour partial pressures, as calculated by Eq. 13.

The first step in the assessment of the dew point is the calculation of the SO_2 concentration in the flue gas. The molar flow of SO_2 stemming from the anode at 100 kA is approximately

$$n^0_{SO_2} = \frac{100 \cdot 10^3}{4F}\frac{M_C}{M_S} \cdot w_S \cdot (1+e) = 0.0970 w_S (1+e) \quad [\text{mols}^{-1}(100\ \text{kA})^{-1}] \tag{12}$$

where F is Faraday's constant [96 485 Asmol^{-1}], M is atomic weight, w_S is the mass fraction of sulfur in the anode, and e is a factor accounting for excess anode consumption (e = 0.13 gives 400 kg C/t Al at 94 % CE).

A part of the SO_2 evolved in the electrolysis cell is adsorbed on the dry scrubber alumina and returned to the cell. The degree of reflux is usually not very far from 0.5. It is not known if the amount of SO_2 refluxed to the cell varies with the draught. The molar flow of SO_2 refluxed with the alumina becomes

$$n_{ref} = n_0 \cdot \frac{\alpha}{1-\alpha} \tag{13}$$

where α is the degree of reflux. Is makes a difference whether the SO_2 is re-evolved from alumina above the crust or from alumina underneath the crust. In the first case, only the SO_2 carried by the air penetrating into the process gas is available for oxidation, while the entire amount of SO_2 is available if the re-evolution takes place underneath the crust. In the following, it will be assumed that the SO_2 is re-evolved from underneath the crust. The amount of SO_2 available for conversion to SO_3 then becomes:

$$n_{\text{available}} = n_0 + n_{ref} = \frac{n_0}{1-\alpha} \tag{14}$$

The concentration of SO_2 is calculated by dividing by the total molar gas flow per 100 kA and correcting for the degree of SO_2 reflux and the concentration of SO_2 in the flue gas:

$$ppmSO_2 = \frac{0.0970 w_S (1+e)}{G_{100} \cdot P^0} RT^0 \cdot \left(\frac{1}{1-\alpha}\right) \cdot 10^6 = \frac{7.828 \cdot 10^6 w_S}{G_{100}} \cdot \frac{1+e}{1-\alpha} \tag{15}$$

where G is the total draught in Nm^{3}h^{-1}(100 kA)$^{-1}$, P^0 is the total pressure ($1.013 \cdot 10^5$ Pa) and T^0 is 273 K. Taking G = 2000 Nm^{3}h^{-1}(100 kA)$^{-1}$, w_S = 0.023, e = 0.13, and α = 0.5, we obtain 203 ppm SO_2 in the flue gas. In the base case, the degree of SO_2 to SO_3 conversion was $1.22 \cdot 10^{-3}$, which gives 0.248 ppm SO_3. With 1 vol% water vapour, corresponding to ambient air at 18 °C and with 60 % relative humidity, the dewpoint becomes 73 °C.

However, the SO_3 formed may also be partly refluxed with the dry scrubber alumina. The treatment is exactly as for refluxed SO_2, and the concentration of SO_3 becomes:

$$ppmSO_3 = ppmSO_2 \cdot \psi \cdot \left(\frac{1}{1-\beta}\right) \tag{16}$$

where β is the degree of SO_3 reflux. The calculated sulfuric acid dewpoint in the base case, assuming different degrees of reflux, is shown in Fig. 10.

It is clear from the present treatment that the dewpoint can vary a lot, although the base case probably represents a quite normal situation. One uncertainty that needs to be resolved is the degree of SO_3 reflux.

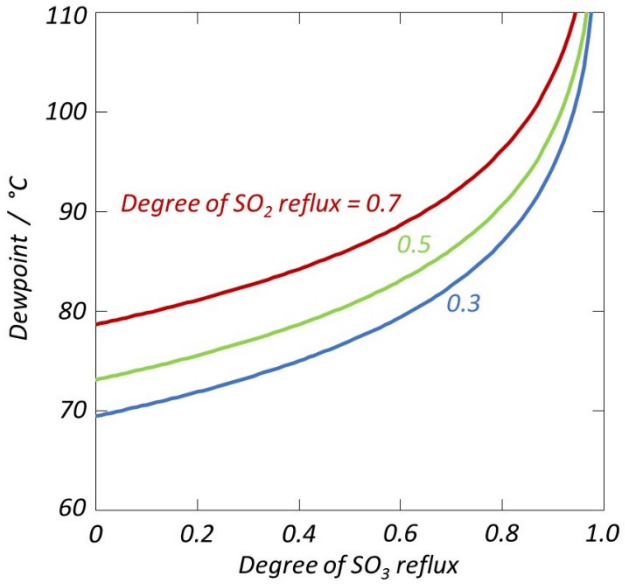

Figure 10. Sulfuric acid dewpoint as a function of the degree of SO_3 reflux at different degrees of SO_2 reflux. Base case with 1 vol% water vapour.

5 Concluding Remarks

The model used in the present work is simplistic. The main uncertainties are probably the conditions in the reaction zone close to the crust opening and the degree of SO_3 reflux. Since the SO_2 to SO_3 conversion is strongly temperature dependent, it would be advantageous to perform CFD modelling of the CO combustion zone and confirm the results by measurements in industrial cells, if possible.

The results obtained in the present works indicates that the degree of SO_2 conversion can vary within wide limits, the current efficiency and the size and number of crust openings being the most important parameters. Recycling of anode gas will involve increasing concentration of SO_2 as well as a slight increase in the H_2O pressure [6]. Before making recommendations concerning the effect on the acid dewpoint, it seems that more information on the reflux of SO_2 and SO_3 from the dry scrubber and their re-evolution from the alumina is needed.

6 Acknowledgement

The present work was supported by HighEFF (Centre for an Energy Efficient and Competitive Industry for the Future), which is a Centre for Environment-friendly Energy Research financed by the Research Council of Norway and numerous end-users; among them Hydro Aluminium, Alcoa, and GE Power.

References

1. S. Broek: Update on SO_2 Scrubbing Applied in Primary Aluminium Smelters, *Light Metals 2020*, 766-776.
2. M. Krämer, M. Schubert, T. Lautensack, T. Hill, R. Körner, F. Rosowski, and J. Zihlke: Catalyst for the Oxidation of SO_2 to SO_3, US Patent No. 8,323,610 B2 (2012).
3. O.-A. Lorentsen, A. Dyrøy, and M. Karlsen: Handling CO_{2eq} from an Aluminum Electrolysis Cell, *Light Metals 2009*, 263-268.
4. G. Wedde: A Method of Ventilating an Aluminium Production Electrolytic Cell, European Patent No. 2,360,296 A1 (2011), US Patent No. 9,458,545 B2 (2016), US Patent No. 9,771,660 B2 (2017).
5. G. Wedde, O.E. Bjarnø, and A.K. Sørhuus: Recycled Pot Gas Distribution, *US Patent US 9 234 286 B2* (2016).
6. A. Solheim and S. Senanu: Recycling of the Flue Gas from Aluminium Electrolysis Cells, *Light Metals 2020*, 803-810.
7. W. Haupin and H. Kvande: Mathematical Model of Fluoride Evolution from Hall-Héroult Cells, *Light Metals 1993*, 257-263.

8. O. Knacke, V.O. Kubaschewski, and K. Hesselmann (Ed.): Thermochemical Properties of Inorganic Substances, 2nd Ed., Springer-Verlag, 1991.
9. T.A. Aarhaug and A.P. Ratvik: Aluminium Primary Production Off-Gas Composition and Emissions: An Overview, *JOM* (2019), https://doi.org/10.1007/s11837-019-03370-6
10. A. Zlochower: Experimental Flammability Limits and Associated Theoretical Flame Temperatures as a Tool for Predicting the Temperature Dependence of these Limits, *J. Loss Prev. Process Ind*. **25**(3) 555-560 (2012).
11. B. Lattimer: Flame Entrainment and Its Application to Compartment Fires, The Ninth International Symposium on Fire Safety Science, Karlsruhe, Germany, 21-26 September 2008 (Proceedings, 883-894).
12. M. Thirumaleshwar: Fundamentals of Heat and Mass Transfer, Dorling Kindersley (India) Pvt. Ltd. (2006).
13. K.S. Osen, T. A. Aarhaug, A. Solheim, E. Skybakmoen, and C. Sommerseth: HF Measurements Inside an Aluminium Electrolysis Cell, *Light Metals 2011*, 263-268.
14. NIST-JANAF Thermochemical Tables, https://janaf.nist.gov/
15. NIST Chemical Kinetics Database, https://kinetics.nist.gov/kinetics/ReactionSearch?r0=7446095&r1=17778802&r2=0&r3=0&r4=0&p0=7446119&p1=0&p2=0&p3=0&p4=0&expandResults=true&
16. G. Wedde: A Method of Ventilating an Aluminium Production Electrolytic Cell, *European Patent EP 2 360 296 A1* (2011), *US Patent US 9 458 545 B2 (2016)*, *US Patent US 9 771 660 B2* (2017).
17. B. ZareNezhad and A. Aminian: Accurate Prediction of the Dew Points of Acidic Combustion Gases by Using an Artificial Neural Network Model, *Energy Conversion and Management* **52**(2) 911-916 (2011).